Real-time Coordinated Trajectory Planning and Obstacle Avoidance for Mobile Robots

Received 23rd July 2010; accepted 25th November 2010.

Lucas C. McNinch, Reza A. Soltan, Kenneth R. Muske, Hashem Ashrafiuon, James C. Peyton

Abstract:

A novel method for real-time coordinated trajectory planning and obstacle avoidance of autonomous mobile robot systems is presented. The desired autonomous system trajectories are generated from a set of first order ODEs. The solution to this system of ODEs converges to either a desired target position or a closed orbit de.ned by a limit cycle. Coordinated control is achieved by utilizing the nature of limit cycles where independent, non-crossing paths are automatically generated from different initial positions that smoothly converge to the desired closed orbits. Real-time obstacle avoidance is achieved by specifying a transitional elliptically shaped closed orbit around the nearest obstacle blocking the path. This orbit determines an alternate trajectory that avoids the obstacle. When the obstacle no longer blocks a direct path to the original target trajectory, a transitional trajectory that returns to the original path is defined. The coordination and obstacle avoidance methods are demonstrated experimentally using differential-drive wheeled mobile robots.

Keywords: *path planning, obstacle avoidance, ODE, mobile robots.*

1. Introduction

A typical method for trajectory planning is to describe the trajectory by a time-varying transitional state variable that converges to the desired target from an arbitrary initial position. A well-defined system trajectory determined in this manner, however, should not have any discontinuities and should admit tracking controller designs that are able to feasibly follow the resulting trajectory. The coordination of a group of autonomous systems is an even more challenging problem because of the potential for dynamic interaction and collision between members of the group and/or obstacles. A number of different approaches for the coordination of a group of autonomous systems into user-defined formations have been proposed. These approaches can be categorized into virtual structure, behavior-based, and leader-follower techniques. A survey of recent research in cooperative control of multi-vehicle systems is presented in [1]. Much of the work in obstacle avoidance has focused on trajectory optimization, decentralized control approaches, behavior-based approaches, and potential .eld methods. A review of path planning and obstacle avoidance techniques is presented in [2] In this work, a novel trajectory planning and obstacle avoidance approach that provides coordinated control of multiple autonomous agents is presented. The proposed strategy is composed of two parts consisting of a coordinated trajec-tory planning algorithm [3] and a real-time obstacle avoid-ance algorithm [4]. The main advantage of this approach is a practical, computationally efficient trajectory planning algorithm with the capability for coordination of multiple autonomous agents and real-time collision avoidance for moving obstacles. To accomplish these tasks, transitional trajectories are defined using sets of ordinary differential equations (ODEs) of two general forms depending on the situation. If the objective is to catch and follow a desired target trajectory, the transitional trajectory is defined by a set of exponentially stable equations whose solution converges to the target trajectory. In the cases of coordinated motion and obstacle avoidance, the trajectory is defined by a set of equations whose solution is a stable limit cycle. A related approach to trajectory planning that is applicable to industrial robot manipulators is presented in [5]. Limit cycles of finite size and shape are used as a way of de.ning complex obstacles to be avoided. Applications of real-time navigation methods for mobile robots using limit cycles have also been addressed in [6], [7]. The limit cycles are defined as circles with constant coef.cients which may result in impractical control demand depending on the distance of the vehicle to the limit cycle. The use of constant coefficients in the limit cycle equations also applies only to stationary limit cycles. In this work, these approaches are expanded to dynamic limit cycles with more general elliptical geometries.

2. Mobile robot platform

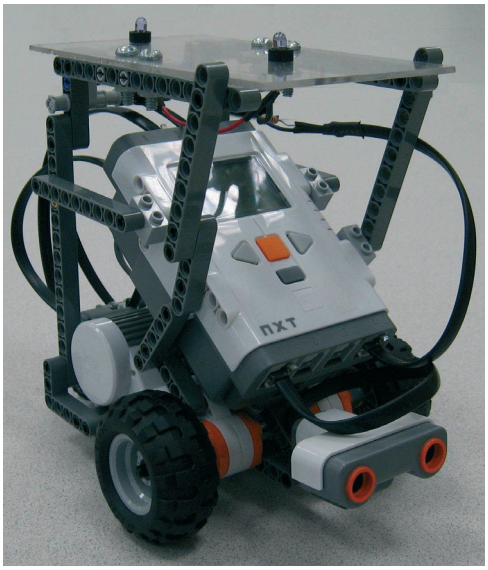

Fig. 1. Experimental mobile robot from each motor to determine the wheel velocities.

The experimental mobile robot system used in this work is the differential-drive wheeled robot shown in Figure 1 based on the LEGO Mindstorms NXT controller. It has the ability for wireless communication between individual robots and a host computer. The coordinated trajectory planning and real-time obstacle avoidance application is developed for this platform in the Matlab/ Simulink programming environment using the ECRobot rapid prototyping development tools [8]. The relatively low cost and high performance of this device results in a very powerful, flexible, and cost-effective mobile computing platform that can be used to implement advanced autonomous system applications directly on the target hardware. Further detail on this mobile robot platform can be found in [9].

A. Kinematic Model

The autonomous mobile robot consists of two indepen-computed using equation (3) and the current position in the dently actuated front drive wheels of radius *r* mounted on inertial reference frame is determined using the kinematic a common axis as shown in Figure 2. The track width *d* represents the length of the segment connecting the wheel centers. A passive caster supports the rear of the mobile robot. The three degree of freedom planar posture of the robot is described in the inertial reference frame by the vector $\mathbf{p} = [x \;\; y \;\; \theta]^T$ and the motion of the mobile robot is subject to the nonholonomic constraint

$$\dot{y}\cos\theta - \dot{x}\sin\theta = 0 \tag{1}$$

arising from the two-dimensional planar kinematics for a differential drive mobile robot. The planar motion is described by the velocity vector $\mathbf{q} = [v \;\; \omega]^T$ where *v* is the forward velocity of the robot in the direction orthogonal to the drive-wheel axis and ω is the angular velocity of the robot about the center of the drive-wheel axis. The kinematic equations relating the body fixed velocities **q** to the inertial reference frame are written as

$$\begin{bmatrix} \dot{x} \\ \dot{y} \\ \dot{\theta} \end{bmatrix} = \begin{bmatrix} \cos\theta & 0 \\ \sin\theta & 0 \\ 0 & 1 \end{bmatrix} \begin{bmatrix} v \\ \omega \end{bmatrix} \tag{2}$$

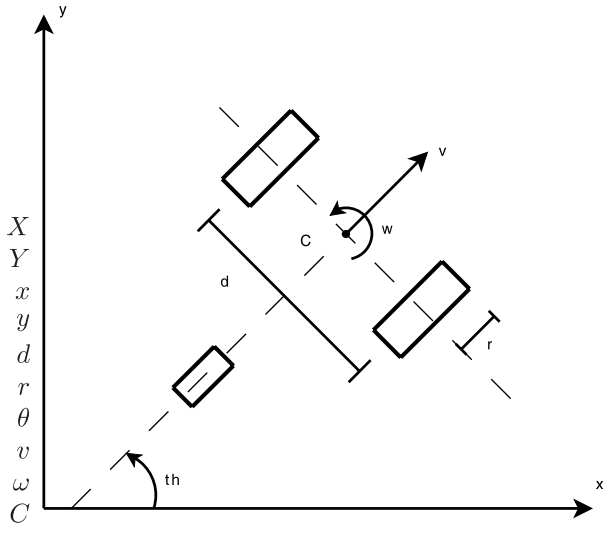

Fig. 2. Differential drive mobile robot schematic.

Assuming there is no wheel slip, the body fixed velocities are related to the angular velocities of the drive wheels by

$$\begin{bmatrix} v \\ \omega \end{bmatrix} = \begin{bmatrix} \frac{r}{2} & \frac{r}{2} \\ \frac{r}{d} & -\frac{r}{d} \end{bmatrix} \begin{bmatrix} \omega_R \\ \omega_L \end{bmatrix} \tag{3}$$

where ω_L and ω_R are the angular velocities of the left and right wheels respectively [10].

B. Position Feedback

Two methods of position feedback are available for the experimental mobile robots. The first uses encoder feedback from each motor to determine the wheel velocities. The current forward velocity *v* and angular velocity ω are then computed using equation (3) and the current position in the inertial reference frame is determined using the kinematic model presented in equation (2). A discrete-time approximation of the current pose of the robot at sample *k* is

$$\mathbf{p}_k = \mathbf{p}_{k-1} + \Delta\mathbf{p}_k = \begin{bmatrix} x_{k-1} \\ y_{k-1} \\ \theta_{k-1} \end{bmatrix} + \begin{bmatrix} Tv_k \cos\left(\theta_{k-1} + \frac{T\omega_k}{2}\right) \\ Tv_k \sin\left(\theta_{k-1} + \frac{T\omega_k}{2}\right) \\ T\omega_k \end{bmatrix} \tag{4}$$

where $\mathbf{p}_k = [x_k \;\; y_k \;\; \theta_k]^T$ and *T* is the sample period.

This method assumes that there is no wheel slip and that the mobile robot travels on a perfectly flat planar surface.

Because there are typically wheel slip and other un measured disturbances present, a more accurate method to determine the robot position based on real-time processing of a camera image is also available. A digital black and white camera mounted a fixed position above the mobile robots is used to view the two infrared LEDs installed at the front and rear of the centerline of the robot as shown in Figure 1. Each camera frame provides a dead reckoning measurement of position and orientation of each robot that is determined from the pixel location of the LEDs [9].

Position measurements are available at approximately are related to the angular velocities of the drive wheels by 20Hz using the camera and at least 100 Hz using the encoders. The advantage of using encoder feedback is that the position can be determined locally without the need to transmit a camera-based position to each robot from the host computer at the 20 Hz sample rate of the camera. The advantage of using camera feedback is that it is a dead reckoning measurement that is not subject to error from wheel slip, uneven surfaces, collisions, and other disturbances. A combination of encoder and camera feedback using multi-rate estimation schemes can be employed to obtain the benefits of each measurement while minimizing the communication requirements, however, this technique is not considered in this work.

C. Local Tracking Control

The reference posture and velocity vectors describing the desired trajectory are defined at each sample period where the reference posture $\mathbf{p}_k^r = [x_k^r \;\; y_k^r \;\; \theta_k^r]^T$ and velocity $\mathbf{q}_k^r = [v_k^r \;\; \omega_k^r]^T$ vectors must adhere to the nonholonomic constraint equation (1). The position and orientation

tracking error vector $\mathbf{e}_k^p = [e_k^x \; e_k^y \; e_k^\theta]^T$ is expressed as

$$\mathbf{e}_k^p = \begin{bmatrix} \cos\theta_k & \sin\theta_k & 0 \\ -\sin\theta_k & \cos\theta_k & 0 \\ 0 & 0 & 1 \end{bmatrix} (\mathbf{p}_k^r - \mathbf{p}_k) \tag{5}$$

where the current pose of the robot is p_k. Various control laws for tracking and position control of mobile robots have been developed. In this work, the following kinematic tracking control law proposed in [11] is used

$$\begin{bmatrix} v_k^s \\ \omega_k^s \end{bmatrix} = \begin{bmatrix} v_k^r \cos e_k^\theta + k_x e_k^x \\ \omega_k^r + v_k^r (k_y e_k^y + k_\theta \sin e_k^\theta) \end{bmatrix} \tag{6}$$

where the tracking errors are defined in equation (5), v_k^s is the corrected forward velocity setpoint, ω_k^s is the corrected angular velocity setpoint and the controller gains k_x, k_y, and k_θ are strictly positive constants. The corresponding wheel velocity setpoints which compensate for any tracking error in the reference trajectory are calculated by inverting equation (3)

$$\begin{bmatrix} \omega_R^s \\ \omega_L^s \end{bmatrix} = \begin{bmatrix} \frac{1}{r} & \frac{d}{2r} \\ \frac{1}{r} & -\frac{d}{2r} \end{bmatrix} \begin{bmatrix} v^s \\ \omega^s \end{bmatrix} \tag{7}$$

where the rotational speed setpoints ω_L^s and ω_R^s are sent to individual wheel speed controllers. An extension of this controller to motor torque and position set point control is proposed in [12].

3. Experimental application

An experimental veri.cation of a novel method of combining trajectory planning and coordination or formation control of robotic and autonomous systems presented in [3] for autonomous surface vessels is demonstrated in this section. The method generates target trajectories that are either asymptotically stable or result in a stable limit cycle. The former case is used to implement formation control. Coordination is guaranteed in the latter case due to the nature of limit cycles where non-crossing independent paths are automatically generated from different starting positions that smoothly converge to closed orbits. A related approach for trajectory planning that is applicable to industrial robot manipulators is presented in [5]. A survey of recent research in cooperative control of multi-vehicle systems is presented in [1].

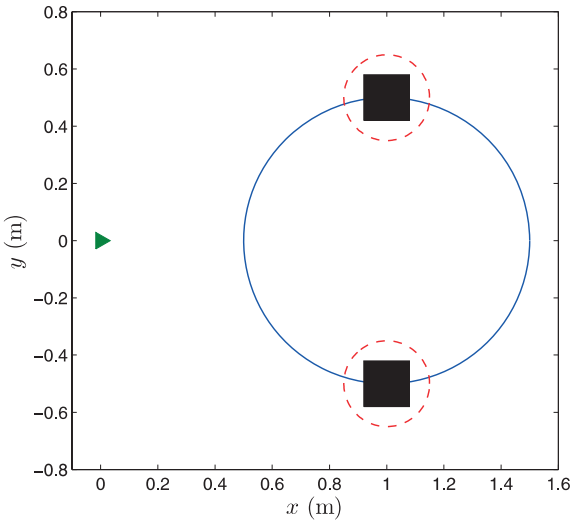

Fig. 3. Trajectory tracking example.

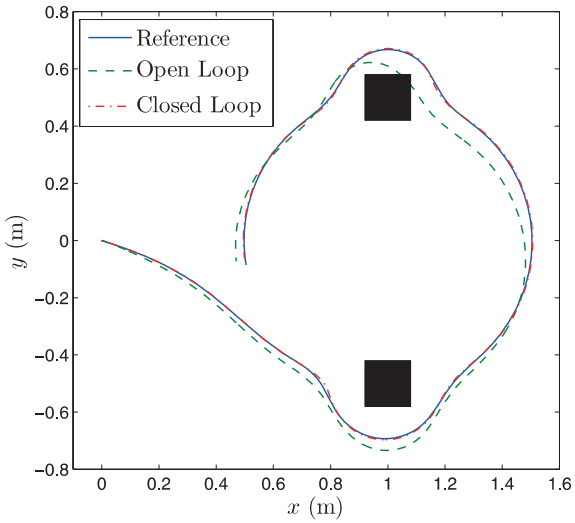

Fig. 4. Open-loop and closed-loop paths.

A. Trajectory Tracking Performance

A demonstration of the mobile robot tracking control performance is provided by defining a reference trajectory that approaches and then follows a circular orbit with a diameter of 1 meter represented by the solid line in Figure 3. The mobile robot must avoid two obstacles in this path that are contained within the circles indicated by the dashed lines in Figure 3. These two circles represent the obstacle boundaries that should not be crossed. Figure 4 presents the desired reference and experimental mobile robot paths with and without tracking control. As shown in this figure, the tracking error increases as the robot turns without encoder feedback tracking control. The maximum tracking error is reduced over five times using the closed-loop tracking control law presented in equation 6. The corresponding tracking errors are presented in Figure 5.

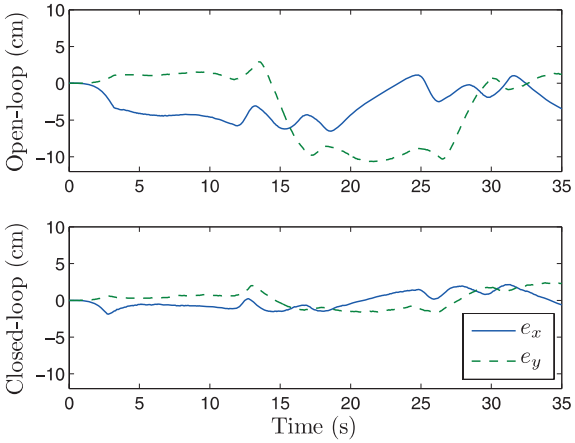

Fig. 5. Trajectory tracking errors.

B. Encoder and Camera Image Position Feedback

Figure 6 compares the desired reference, encoder, and camera image paths for the mobile robot under tracking control using encoder feedback on a flat surface with minimal wheel slip. As shown in this figure, there is very little difference between the position determined from the en coders and that determined from the camera image. Figure 7 presents a similar scenario except there is significant wheel slip obtained by using plastic wheels, as opposed to rubber, on a slick surface and specifying

a trajectory with a smaller turning radius. A large error in the encoder position is now present under these conditions. In the sequel, the conditions in Figure 6 are used such that encoder feedback will provide an acceptable position measurement. The advantage of en coder feedback is that the position can be determined locally by each robot without the need to transmit a camera-based position to each robot at the 20 Hz sample rate of the wheel speed controllers.

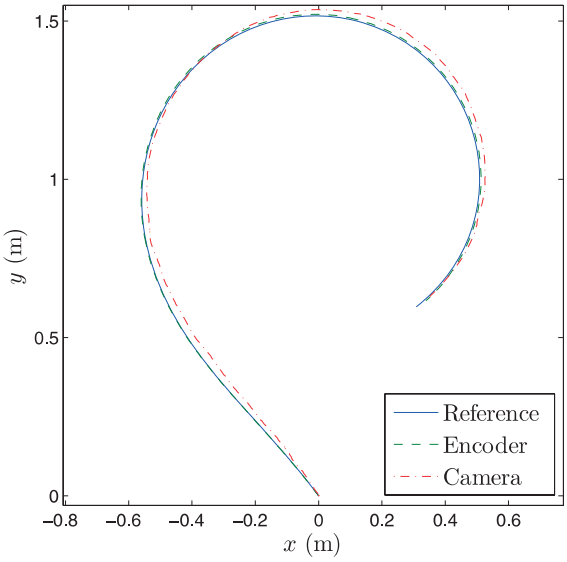

Fig. 6. Closed-loop trajectory with camera position.

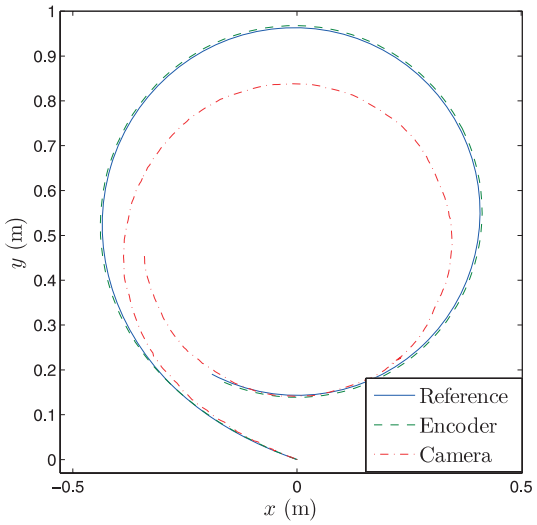

Fig. 7. Closed-loop tracking error with slip.

C. Reference Trajectory Determination

The reference trajectory for each mobile robot is defined using a set of two ordinary differential equations (ODEs) in terms of the two planar global position variables x and y

$$\dot{x}_i = f_i(x_1, x_2, t), \;\; f_i : D_i \to \mathbb{R}^2, \;\; i = 1, 2 \tag{8}$$

where x_1 and x_2 are the state variables, D_i is an open and connected subset of $\mathbb{R}^2$, and f_i is a locally Lipschitz map from D_i into $\mathbb{R}^2$. The state variables x_1 and x_2 are defined as

$$\begin{aligned} x_1 &= x^r - x^* \\ x_2 &= y^r - y^* \end{aligned} \tag{9}$$

where the definition of x^* and y^* and the form of the functions f_1 and f_2 are determined based on the type of reference trajectory. The reference posture $\mathbf{p}^r$ and velocity $\mathbf{q}^r$ are obtained from the state variables by

$$\mathbf{p}^r = \begin{bmatrix} x^r \\ y^r \\ \theta^r \end{bmatrix} = \begin{bmatrix} x_1 + x^* \\ x_2 + y^* \\ \arctan\left(\dfrac{\dot{x}_2 + \dot{y}^*}{\dot{x}_1 + \dot{x}^*}\right) \end{bmatrix} \tag{10}$$

$$\mathbf{q}^r = \begin{bmatrix} v^r \\ \omega^r \end{bmatrix} = \begin{bmatrix} \sqrt{(\dot{x}^r)^2 + (\dot{y}^r)^2} \\ \dfrac{1}{v^r}(\ddot{y}^r \cos\theta^r - \ddot{x}^r \sin\theta^r) \end{bmatrix} \tag{11}$$

where the expressions for θ^r and ω^r arise from the nonholonomic constraint in equation (1)

Two general types of reference trajectory are presented in this work. The first is implemented when the mobile robot is required to reach a target position which may be either moving or stationary. This type of reference trajectory is referred to as a *Transitional Target Trajectory*. The second is implemented when the mobile robot is required to smoothly converge to and then follow a closed orbit. This type is referred to as a *Transitional Limit Cycle Trajectory*.

D. Transitional Target Trajectory

The transitional target trajectory defines a reference trajectory for which the mobile robot path converges exponentially to a stationary or moving target position. The desired reference position is denoted by $x^r(t)$ and $y^r(t)$ and the target position is denoted by $x^t(t)$ and $y^t(t)$ in the inertial reference frame. The state variables introduced in equation (9) are defined as

$$\begin{aligned} x_1 &= x^r - x^t \\ x_2 &= y^r - y^t \end{aligned} \tag{12}$$

such that when the ODEs in equation (8) are asymptotically or finite time stable, $x_1(t), x_2(t) \to 0$, which implies that $x^r \to x^t(t)$ and $y^r \to y^t(t)$.

The exponentially stable transitional target trajectory used in this work is defined by the following linear ODE system

$$\begin{aligned} \dot{x}_1 &= -k_1 x_1 \quad k_1(t) > 0 \\ \dot{x}_2 &= -k_2 x_2 \quad k_2(t) > 0 \end{aligned} \quad t \geq t_0 \tag{13}$$

where t_0 is the initial time. The strictly positive parameters $k_1(t)$ and $k_2(t)$ are assumed to be functions of time in order to generate desired reference trajectories that conform to the physical constraints of the mobile robot system. In general, they are selected as monotonically increasing positive time functions that start from a small value and are defined based on actuator limitations and the distance to the target. Fifth order polynomials allow for smooth and monotonic transitions of these parameters to their final values. The following polynomial may be used to compute each parameter k_i, i=1,2 during the transition period $t_0 \leq t \leq t_1$

$$k_i = k_{i5}\Delta t^5 + k_{i4}\Delta t^4 + k_{i3}\Delta t^3 + k_{i2}\Delta t^2 + k_{i1}\Delta t + k_{i0} \tag{14}$$

where $\Delta t = t - t_0$. The following boundary conditions are selected to smoothly increase the value of k_i from 1% to 100% of its final value k_i

$$k_i(t_0) = \bar{k}_i/100,\ \ k_i(t_1) = \bar{k}_i,$$
$$\dot{k}_i(t_0) = \dot{k}_i(t_1) = \ddot{k}_i(t_0) = \ddot{k}_i(t_1) = 0 \tag{15}$$

where $\dot{k}_i$ and $\ddot{k}_i$ are the 1st and 2nd time derivatives of k_i. The six polynomial coefficients k_{ij}, j = 0,...,5 are derived using the six boundary conditions specified in equation (15). Note that $k_i = \bar{k}_i$ if or $t > t_1$ and t_1 is selected based on the initial distance of the target from the vessel.

E. Transitional Limit Cycle Trajectory

The transitional limit cycle trajectory defines a globally exponentially stable limit cycle to which the desired reference trajectory will converge. The state variables introduced in equation (9) for the transitional limit cycle trajectory are defined as

$$x_1 = x^r - x^o$$
$$x_2 = y^r - y^o \tag{16}$$

where $x^o(t)$and $y^o(t)$denote the position of the origin of the limit cycle in the inertial reference frame. The origin of the limit cycle is assumed to be a function of time to allow for dynamic obstacles. The transitional limit cycle trajectory has the following form

$$\dot{x}_1 = h_1(x_1, x_2, t) - k_1 x_1 l(x_1, x_2, t), \quad k_1(t) > 0$$
$$\dot{x}_2 = h_2(x_1, x_2, t) - k_2 x_2 l(x_1, x_2, t), \quad k_2(t) > 0 \tag{17}$$

where $l(x_1,x_2,t)$ defines the limit cycle geometry which may be an explicit function of time to account for obstacle planar rotation. The functions $h_1(x_1,x_2,t)$ and $h_2(x_1,x_2,t)$ represent the planar particle motion kinematics on the limit cycle; i.e. when $l(x_1,x_2,t) = 0$. The solution of equation (17) guarantees that any trajectory with an initial position outside of the limit cycle will converge to the limit cycle without crossing it. The positive parameters $k_1(t)$ and $k_2(t)$ are again assumed to be functions of time in order to generate realizable trajectories and are derived using equation (14).

F. Elliptical Limit Cycles

In this work an elliptical limit cycle geometry is used. This is a very general shape which can be used for obstacle avoidance, coordinated control, aerial coverage or any number of other trajectory planning applications. The limit cycle $l(x_1,x_2,t)$ is defined by the general equation of an ellipse with semi major and semi minor axes, a and b, respectively, and origin at $(x^o(t),y^o(t))$

$$l(x_1, x_2, t) = \left[\frac{\cos\phi x_1 + \sin\phi x_2}{a}\right]^2 + \left[\frac{-\sin\phi x_1 + \cos\phi x_2}{b}\right]^2 - 1 \tag{18}$$

where $x_1(t)$ and $x_2(t)$ are defined in equation (16) and $\phi(t)$ is the angle representing the orientation of the ellipse semi major axis relative to the global horizontal axis. This angle can be time dependent if the desired limit cycle is rotating. The functions $h_1(x_1,x_2,t)$ and $h_2(x_1,x_2,t)$ are defined based on the motion of a particle around an ellipse

$$x_1 = a\cos\phi\cos\Omega t - b\sin\phi\sin\Omega t$$
$$x_2 = a\sin\phi\cos\Omega t + b\cos\phi\sin\Omega t \tag{19}$$

where $\Omega(t)$ is the average angular velocity of the particle on the limit cycle. Note that $\Omega(t) > 0$ represents counter-clockwise (CCW) rotation and $\Omega(t) < 0$ represents clockwise (CW) rotation. The time derivative of equation (19) is

$$\dot{x}_1 = -(\Omega + \dot{\Omega}t)(a\cos\phi\sin\Omega t + b\sin\phi\cos\Omega t) - x_2\dot{\phi}$$
$$\dot{x}_2 = (\Omega + \dot{\Omega}t)(-a\sin\phi\sin\Omega t + b\cos\phi\cos\Omega t) - x_1\dot{\phi} \tag{20}$$

where $\dot{\Omega}$ is the time derivative of Ω. The functions $h_1(x_1,x_2,t)$ and $h_2(x_1,x_2,t)$ are derived by eliminating cosΩt and sinΩt from equations (19) and (20) and are given by

$$h_1(x_1, x_2, t) = \dot{x}_1 = -x_2\dot{\phi} + \frac{\Omega + \dot{\Omega}t}{ab}(h_{e11}x_1 - h_{e12}x_2)$$
$$h_2(x_1, x_2, t) = \dot{x}_2 = +x_1\dot{\phi} + \frac{\Omega + \dot{\Omega}t}{ab}(h_{e21}x_1 - h_{e11}x_2) \tag{21}$$

where

$$h_{e11} = (a^2 - b^2)\sin\phi\cos\phi$$
$$h_{e12} = a^2\cos^2\phi + b^2\sin^2\phi \tag{22}$$
$$h_{e21} = b^2\cos^2\phi + a^2\sin^2\phi.$$

The average angular velocity $\Omega(t)$ is assumed to be monotonically increasing in magnitude such that $\Omega+\dot{\Omega} \neq 0$. Again, a fifth order polynomial is used to transition $\Omega(t)$ from 1% to 100% of its final constant value $\bar{\Omega}$ in the selected transition period of $t_0 \leq t \leq t_1$

$$\Omega = \Omega_5\Delta t^5 + \Omega_4\Delta t^4 + \Omega_3\Delta t^3 + \Omega_2\Delta t^2 + \Omega_1\Delta t + \Omega_0 \tag{23}$$

where $\Delta t = t - t_0$. The following boundary conditions

$$\Omega(t_0) = \bar{\Omega}/100,\ \ \Omega(t_1) = \bar{\Omega},$$
$$\dot{\Omega}(t_0) = \dot{\Omega}(t_1) = \ddot{\Omega}(t_0) = \ddot{\Omega}(t_1) = 0 \tag{24}$$

are used to derive the six polynomial coefficients Ω_i, i=0,...,5.

4. Coordinated control

An application of the transitional limit cycle trajectory is coordinated control. The trajectories defined in equation (17), which converge to stable limit cycles, are ideal for co-ordinated control because all paths to the limit cycle are independent and non-crossing due to the uniqueness of the solution to the ODEs. The following experimental example considers the coordinated motion of three identical mobile robots that join an elliptical reference trajectory at spaced intervals and maintain the elliptical motion. The mobile robots are initially located at the (x,y) positions (–1,0), (0.5,0.5), and (0.5,–0.5) expressed in meters. Each robot joins the elliptical reference trajectory with semi-major and semi-minor axes of a=0.5m and b=0.3m respectively oriented with ϕ=–30degrees, its center at (0,0) and a desired angular velocity of Ω=0.45rad/sec. The final values of the trajectory parameters are selected as $\bar{k}_1 = \bar{k}_2$=0.8. Figure 8 presents the actual trajectories of the three mobile robots under tracking control using encoder feedback. The trajectories shown remain within 2 cm of the desired reference trajectory for the duration of the experiment. The markers on each trajectory represent the mobile robot positions at 2.5 second intervals for the first ten seconds of the trajectory. The velocities during the initial portion of the trajectory as the mobile robot joins the limit cycle depend on the initial distance from the closed orbit. Robots that start closer to the closed orbit proceed at a slower velocity while those that start further

away must approach at a higher velocity such that all three robots converge to the limit cycle in the proper orientation. Note that these velocities are automatically generated by the ODEs in equation (17). The trajectories presented in figure 8 are calculated based on the encoder feedback used by the control law. However, because of wheel slip, changes in elevation of the ground surface and/or other external disturbances, the trajectory that the robot actually follows may be different from that calculated based on encoder feedback. Figure 9 presents the reference and actual trajectories of the robot which started at (1.5,0.5), including the camera image trajectory. This .gure shows that, in contrast with the trajectory presented in Figure 6, under some circumstances, the actual trajectory of the mobile robot using encoder-based feedback may deviate from the desired reference trajectory. It may become necessary to include the camera image feedback in the tracking control law when this deviation becomes significant.

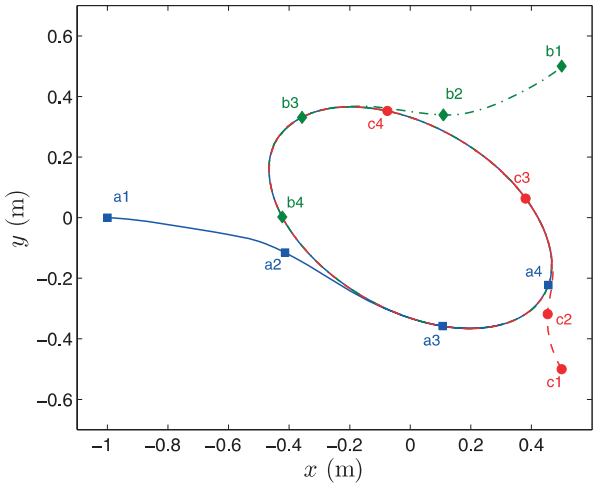

Fig. 8. Experimental coordinated robot trajectories.

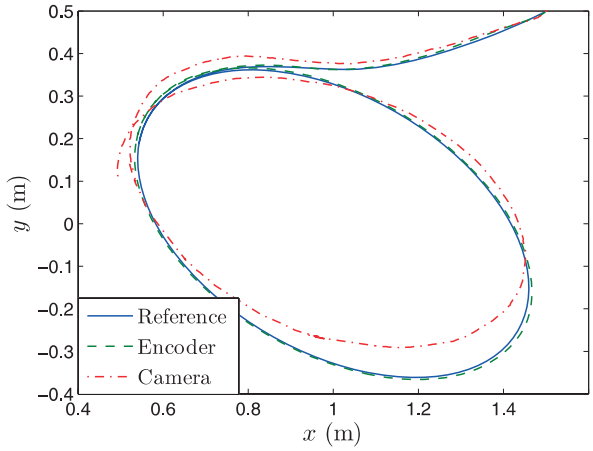

Fig. 9. Elliptical trajectory with camera position data.

5. Obstacle avoidance

An application of both the transitional limit cycle and transitional target trajectories is the problem of obstacle avoidance. In this application, a mobile robot is commanded to converge on a target position in the presence of several stationary or moving obstacles. The obstacles can be approximated by elliptical limit cycles as developed in section III-F. At each sample time, the nearest obstacles on a straight line path from the mobile robot to its target is detected. Real-time obstacle avoidance is carried out by transitioning from the target tracking trajectory to a trajectory that approaches the nearest obstacle in the original path. As soon as the mobile robot is around the obstacle, the trajectory is switched either to another limit cycle approximating and enclosing the next obstacle or to the original target-tracking trajectory. In the following experimental example the mobile robot starts at the origin and its target position is (1.5,0). Obstacles are located at (0.5,0) and (1,-0.1)and are approximated by circular limit cycles with radius r=0.15. Figure 10 shows the desired reference, encoder, and camera image paths for the robot under tracking control with encoder feedback. The numbered markers along the desired reference trajectory represent the desired positions at four different times. Marker 1 represents the initial position of the mobile robot and marker 4 represents the target position. At the first instant of the experiment, the obstacle avoidance algorithm recognizes that obstacle 1 is the closest obstacle lying in the straight line path to the target and a transitional limit cycle trajectory surrounding the obstacle is generated. The mobile robot approaches obstacle 1 following the transitional limit cycle trajectory until the next obstacle is detected in its path. A new transitional limit cycle trajectory is generated beginning at at marker 2. This trajectory is followed until marker 3 at which point the obstacle no longer lies in the direct path to the target. Finally, the transitional target trajectory de.ned in Section III-D is used to converge on the .nal target position.

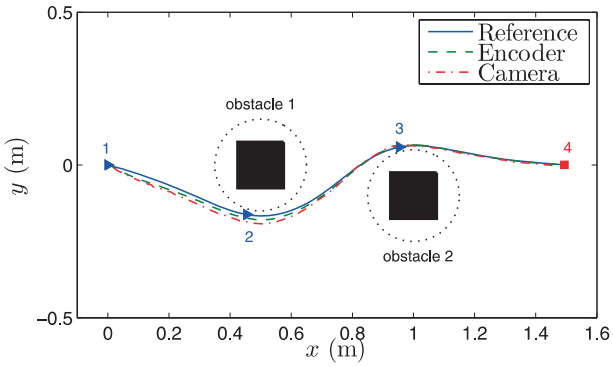

Fig. 10. Experimental obstacle avoidance trajectories.

6. Conclusions

A novel method combining coordinated control and real-time obstacle avoidance for autonomous systems is presented and experimentally veri.ed using mobile robots. The method generates transitional reference trajectories as a function of the current system trajectory and the desired target trajectory. The method can be used for coordinated control of several robots guaranteeing unique collision free paths and coordi-nated operation. It can also be used for real-time obstacle avoidance and target tracking applications.

ACKNOWLEDGMENTS
Support for this work from the Of.ce of Naval Research under ONR Grant N00014-04-1-0642, the National Science Foundation under NSF Grant DUE-0837637, and the Center for Nonlinear Dynamics and Control (CENDAC) at Villanova University is gratefully acknowledged.

AUTHORS
Lucas C. McNinch*, Reza A. Soltan, Kenneth R. Muske, Hashem Ashrafiuon, James C. Peyton Jones - Center for Nonlinear Dynamics and Control Villanova University, Villanova, PA 19085 USA. E-mails: lucas.mcninch@villanova.edu, reza.aliakbarsoltan@villanova.edu, kenneth.muske@villanova.edu, hashem.ashrafiuon@villanova.edu, james.peyton-jones@villanova.edu.
* Corresponding author

References

[1] R. Murray. Recent research in cooperative control of multivehicle systems. *Journal of Dynamic Systems, Measurement, and Control*, 2007, 129(5), pp. 571-583.

[2] V. Kunchev, L. Jain, V. Ivancevic, A Finn. Path planning and obstacle avoidance for autonomous mobile robots: A review. In: *Proc. of the 10th International Conference on Knowledge-Based Intelligent Information and Engineering Systems, volume 4252 of Lecture Notes in Artificial Intelligence*, Springer-Verlag, 2006, pp. 537-544.

[3] R. Soltan, H. Ashra.uon, K. Muske. Trajectory planning and coordinated control of robotic systems. In: *Proc. of the 2009 ASME IDETC/CIE Conference*, 2009.

[4] R. Soltan, H. Ashrafiuon, K. Muske. Trajectory real-time obstacle avoidance for underactuated unmanned surface vessels. In: *Proc. of the 2009 ASME IDETC/CIE Conference*, 2009.

[5] L.P. Ellekilde, J. Perram. Tool center trajectory planning for industrial robot manipulators using dyna-mical systems. *The International Journal of Robotics Research*, 2005, 24(5), pp. 385-396.

[6] D.H. Kim, J.H. Kim. A real-time limit-cycle navigation method for fast mobile robots and its application to robot soccer. *Robotics and Autonomous Systems*, 2003, 42(1), pp. 17-30.

[7] R. Grech, S.G. Fabri. Trajectory tracking in the presence of obstacles using the limit cycle navigation method. In: *Proc. of the 20th IEEE International Symposium on Intelligent Control and the 13th Mediterranean Conference on Control and Automation*, 2005, pp. 101-106.

[8] T. Chikamasa. Embedded coder robot NXT instruction manual, 2009. www.mathworks.com/matlabcentral/fileexchange/ 13399/.

[9] L. McNinch, R. Soltan, K. Muske, H. Ashrafiuon, J. Peyton Jones. An experimental mobile robot platform for autonomous systems research and education. In: *Proc. of the 14th IASTED International Conference on Robotics and Applications*, in press, 2009.

[10] G. Antonelli, S. Chiaverini, G. Fusco. A calibration method for odometry of mobile robots based on the least-squares technique: Theory and experimental validation. *IEEE Transactions on Robotics*, 2005, 21(5), pp. 994-1004.

[11] Y. Kanayama, Y. Kimura, F. Miyazaki, T. Noguchi. A stable tracking control method for an autonomous mobile robot. In: *Proc. of the 1990 IEEE International Conference on Robotics and Automation*, 1990, pp. 384-389.

[12] R. Fierro, F. L. Lewis. Control of a nonholonomic mobile robot: Backstepping kinematics into dynamics. *Journal of Robotic Systems*, 1997, 14(3), pp. 149-163.